NONLINEARITY OF DEGENERATELY DOPED FLEXURAL MODE SILICON MICROMECHANICAL RESONATORS

Saisneha Koppaka[1], Anne L. Alter[1], Gabrielle D. Vukasin[1], Dongsuk D. Shin[1], Ian B. Flader[1], Yunhan Chen[2], and Thomas W. Kenny[1]*
[1]Stanford University, Stanford, California, USA
[2]Apple Inc., Cupertino, California, USA

ABSTRACT

In this paper, we present an experimental study of nonlinearities in degenerately doped flexural-mode silicon MEMS resonators. Two geometries (single and double-anchored) and two wafer orientations (<100> and <111>) are used to analyze the elastic effects of p-type (1.31×10^{16} to 1.61×10^{15} cm^{-3}) and n-type (1.264×10^{15} to 2.64×10^{14} cm^{-3}) degenerately doped double-ended tuning forks. We employ closed-loop frequency sweeps to characterize the amplitude-frequency response of each system. Experimental results show that geometric nonlinearities and electrostatic nonlinearities dominate material and crystalline orientation-dependent nonlinearities in the flexural mode. These results present an initial exploration into characterizing nonlinear mechanical behavior of resonators operating in lower frequency bending modes.

KEYWORDS

Flexural mode resonator; nonlinear oscillators; degenerate doping; geometric nonlinearity

INTRODUCTION

Electrostatically actuated microelectromechanical (MEMS) oscillators have become a successful alternative to quartz crystal as they provide benefits such as compatibility with on-chip CMOS circuitry and size reduction for commercial applications [1]. The reduced device size and mass, however, comes with the drawback of lower power handling capability and smaller output capacitances. As the resonator is driven to larger amplitudes to overcome the reduced signal-to-noise ratios, devices can enter the nonlinear region where the amplitude-dependent higher order terms can dominate system behavior [2]. Duffing nonlinearities and nonlinear dissipation are examples of parameters that become more significant.

Conservative nonlinearities can be broadly categorized as electrostatic nonlinearities and mechanical (geometric, material, orientation) nonlinearities [3]. Previous studies have characterized the nonlinearities of doped bulk mode resonators [4], including the material nonlinear limits of Lamé resonators [5] nonlinearity in n-type doped silicon resonators [6], and analytical models of the nonlinear Young's modulus [7]. Work on the flexural mode resonators has been limited because of the generally high feedthrough effects at larger input voltages. This work focuses on double-ended tuning fork (DETF) resonators that have been characterized as temperature references and well-studied for their dissipative nonlinearities [8]. The potential reduction in the frequency-temperature coefficient for silicon MEMS makes degenerately doped silicon resonators an especially interesting device family of study. Figure 1 shows the two kinds of DETFs utilized in our study: single-anchored (SA) and double-anchored (DA) with the flexural mode resonant frequency at an average of 1.10 MHz for SA-DETFs and 1.12 MHz for DA-DETFs. These two devices provide a contrasting comparison since the addition of the second anchor increases the overall strain in the device, which can bring geometric stiffening nonlinearities into play. All devices in this work were fabricated in the epi-seal encapsulation process [9] [10] with varying doping levels and orientations as labeled in the following figures.

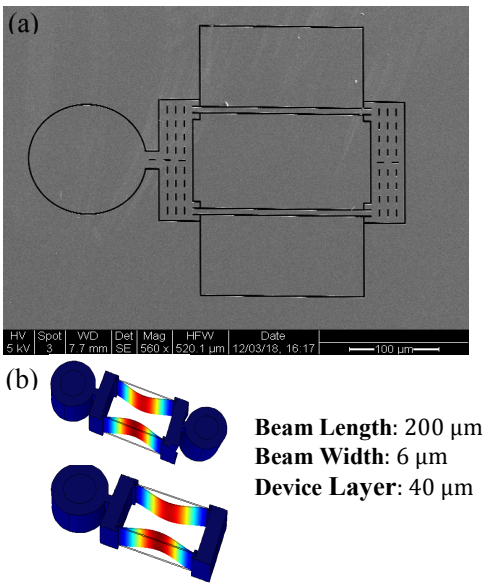

Figure 1: (a) SEM of DETF device (top-down view) and (b) The COMSOL model of a SA (bottom) and DA (top) DETF device operating in the symmetric flexural mode.

The table below summarizes the resistivity and doping concentration information for p-type and n-type dopants in on <100> and <111> wafers. This also summarizes the array of devices we present in this study.

Table 1: Resistivity and dopant concentration for p-type and n-type dopants on <100> and <111> wafers.

Dopant	**Resistivity ($m\Omega - cm$)**	**Concentration (cm^{-3})**
Boron	<100> : 1.13 <111 > : 8.47	<100>:1.31×10^{16} <111>:1.61×10^{15}
Antimony	<100> : 3.66 <111 >: 17.0	<100>:1.36×10^{15} <111>:2.64×10^{14}

THEORY

The dynamics of the vibrational mode of a nonlinear MEMS resonator can be modeled as a single-degree of freedom lumped mass system with an equation of motion:

$$m\ddot{x} + c\dot{x} + k_0 x + k_1 x^2 + k_2 x^3 = F\cos(\omega t) \quad (1)$$

where x is the modal displacement, m is the lumped mass, c is the linear damping coefficient, k_0 is the linear spring constant, k_1 and k_2 represent higher order nonlinear spring constants, and F is the magnitude of the external periodic input drive to the system. The system's linear natural frequency is defined as $\omega_0 = \sqrt{k_0/m}$.

The analytical frequency response results referenced from [11] and [12] describe the change in the resonant frequency (f) as a function of the change in amplitude (a) in the presence of a given nonlinearity.

$$f \cong f_0 + \kappa a^2 \rightarrow \kappa = \Delta f / a^2 \quad (2)$$

The resulting ratio (κ) is the amplitude-frequency coefficient of the system (A-f coefficient) and it can be estimated with the first and the second order anharmonic stiffness coefficients. The magnitudes and polarities of stiffness coefficients k_0, k_1, k_2 predict the shift in the resonance peak either towards the lower frequencies ("softening") or towards the higher frequencies ("hardening").

$$\kappa = \left(\frac{3}{8}\frac{k_2}{k_0} - \frac{5}{12}\frac{k_1^2}{k_0^2}\right) f_0 \quad (3)$$

Mechanical nonlinearities are the result of either intrinsic properties of the crystal lattice or additional kinematic effects resulting from changes to the stress-strain distribution. The effect of these nonlinearities can be described by the nonlinear engineering Young's modulus for a resonator body subject to large deformations:

$$E = E_0 + E_1\epsilon + E_2\epsilon^2 \quad (4)$$

where ϵ is the engineering strain, E is the effective Young's modulus, E_0 is the linear Young's modulus, and E_1 and E_2 are the higher order correction terms due to the large strain factor. The contribution of free electrons on the second and third order elastic constants for n- and p-type silicon can be used to analytically compute the nonlinear engineering Young's modulus.

Electrostatic nonlinearities, on the other hand, arise from the variable gap capacitive transduction and are a function of the electrode and resonator configuration. The analytical model from Yang *et. al* estimate the first order electrostatic spring constant shift in resonant frequency as a function of bias voltage,

$$f_0 \cong \frac{1}{2\pi}\sqrt{\frac{1}{m}\left(k_0 - \frac{N\varepsilon_0 V_b^2 A}{d_0^3}\right)} \quad (5)$$

where N is the total number of electrodes, V_b is the dc bias voltage and d_0 is the initial transduction gap size, and A is the transduction area. Equation 5 demonstrates that the resonant frequency is a function of the bias voltage; specifically, increasing the bias voltage shifts the linear resonant frequency to lower frequencies.

CHARACTERIZATION METHOD AND EXPERIMENTAL RESULTS

The experimental setup used to perform closed loop frequency sweeps is included in Figure 2. To prepare the resonator for testing, encapsulated epi-seal devices are mounted to a printed circuit board via a chip carrier, wire bonded to the package, and placed in an environmental control chamber at 30 ± 0.1 °C for temperature control. The ac output signal from a Zurich HF2LI lock-in amplifier excites the resonator while the resonator body remains biased at a constant dc voltage of 35 V. The resonator output current is converted into a voltage using a trans-impedance amplifier (TIA). By maintain a variable-phase feedback loop on the resonator, we can track the amplitude as a function of frequency of the resonator beyond the critical bifurcation regime [13].

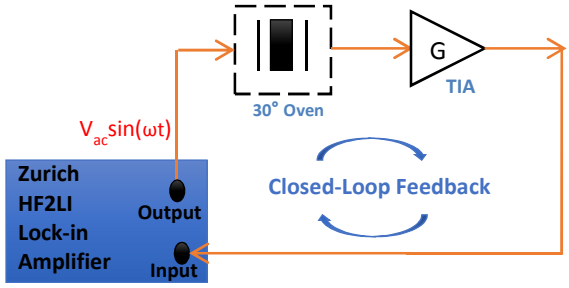

Figure 2: Experimental apparatus used for closed loop frequency sweep measurements

The resonator displacement a is estimated as a first order approximation from the output voltage of the TIA (V_{out}) scaled by the gain of the TIA (G_{tot}):

$$a \cong \frac{V_{out} d_0^2}{2\pi f_0 G_{tot} V_b \varepsilon_0 A} \quad (6)$$

Figure 3 shows the closed-loop frequency response for resonators of different doping and wafer orientation. Each color represents increasing input ac drive voltage to the resonator from low drive (blue) to high drive voltages (red).

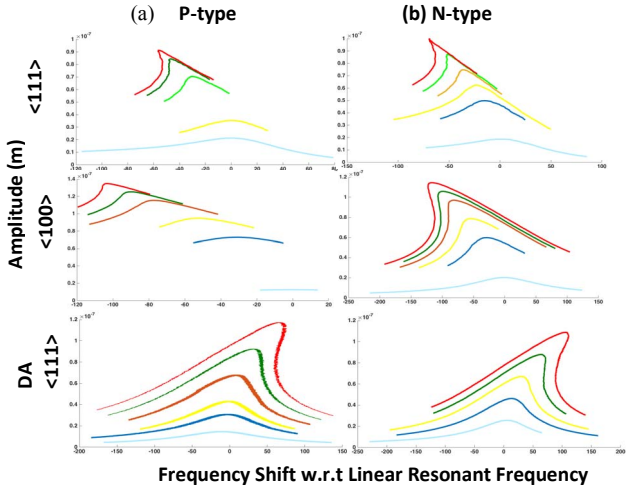

Figure 3: Closed loop frequency sweeps of (a) p-type (b) n-type wafers of two different orientations. The top two rows are sweeps of SA-DETFs and the bottom row are sweeps of DA-DETFs.

SA-DETFs on both <100> <111> wafers exhibit a softening nonlinearity regardless of doping while DA-DETFs on <111> wafers exhibit a hardening nonlinearity regardless of dopant-type.

From the closed-loops measurements, the value of the amplitude-frequency coefficient κ can be calculated through tracking the maximum vibrational amplitude and determining the corresponding frequency shift, measured in hertz, with respect to the linear resonant frequency. The results are then fit with Equation 2 and plotted in Figure 4.

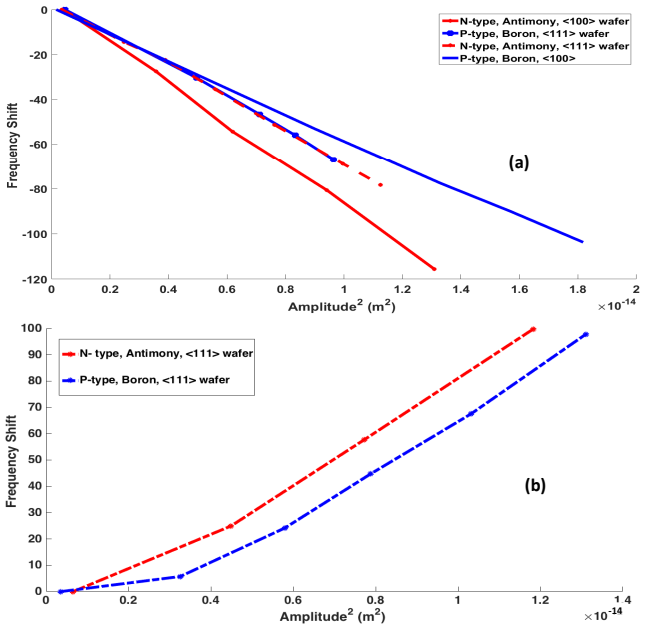

Figure 4: (a) Combined plots of the amplitude-frequency coefficients for SA DETFs of various doping and wafer orientation (b) Combined amplitude-frequency coefficients for DA DETFs of various doping. Frequency shift is measured in Hz as the difference from the linear resonant frequency.

We explore the repeatability our data set due to external factors including the variability in a DETF on the same die oriented in the 0° versus 90° direction, reticle to reticle variability, variability due to wire-bonding of the die to the printed circuit board, and variability due to die thickness. To explore the die thickness variability, a die was thinned to a total thickness of 150 μm and compared to a non-thinned die on the same wafer. Figure 5 represents the reticle to reticle variability for both SA and DA-DETFs while Figure 6 shows that repeatability is independent of external factors. In Figure 6 (b) and 6 (c) the run to run variability refers to obtaining the same set of data multiple times to understand errors due to oven temperature fluctuations, lock-in frequency drift, and any other environmental changes. These results all confirm that the SA-devices are dominated by the electrostatic softening nonlinearity while the DA-devices are dominated by the geometric hardening nonlinearity, and the materials effects are secondary.

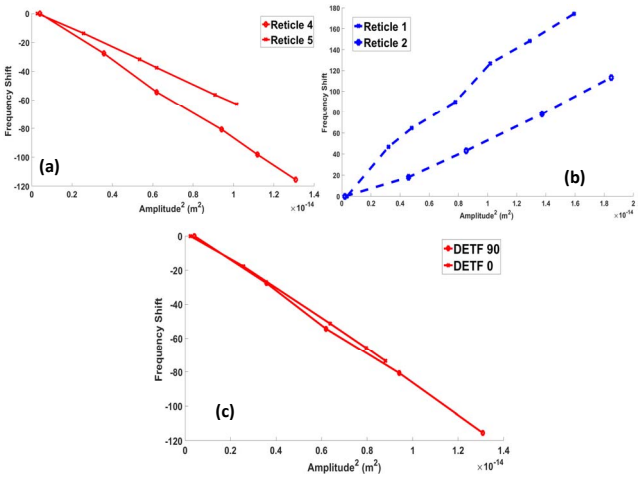

Figure 5: Reticle-to-reticle variability of the amplitude-frequency coefficient for (a) N-type, Antimony, <100>, SA-DETF (b) P-type, <111> wafer, DA-DETF and (c) for a DETF on a given wafer, variability due to the 0 deg and 90 deg orientation.

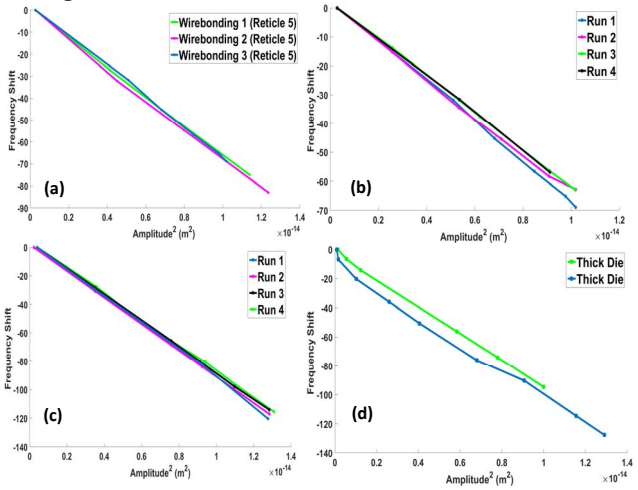

Figure 6: Experimental repeatability independent of external factors including (a) wirebonding (b) run-to-run variation on the N-type, Antimony SA-DETF on reticle 5 (c) run-to-run variation on the N-type, Antimony, SA-DETF from HDXIII on reticle 4 (d) thick vs. thinning of the die

CONCLUSIONS

Experimental results show that electrostatic and geometric nonlinearities dominate any material-dependent nonlinear effects for flexural mode resonators. We observe high consistency between data set to data set, wire-bonding, and devices on the same reticle. However, the variability between two different reticles, which is on the same order magnitude as the variability due to doping suggests that we cannot, at this time, quantify the amplitude-frequency coefficients for a specific geometry and doping. This work will continue with careful exploration of nonlinearities in other MEMS flexural resonators, such as disk gyroscopes, which operate with similar flexural modes.

ACKNOWLEDGEMENTS

This work was supported by the Defense Advanced

Research Projects Agency (DARPA) grant "Precise Robust Inertial Guidance for Munitions (PRIGM)", managed by Dr. Ron Polcawich, Contract Number #N66001-16-1-4023. This was work performed in part at the Stanford Nanofabrication Facility (SNF) supported by the National Science Foundation under Grant ECS-9731293. Special thanks to all the SNF staff for their help during the fabrication process.

REFERENCES

[1] SiTime.Inc. MHz Oscillators, accessed Feb 2019. [Online]. Available: www.sitime.com/products/mhz-oscillators

[2] M. Youni, "MEMS Linear and Nonlinear Statics and Dynamics," New York, NY, USA: Springer, 2011.

[3] Y.Yang, E.J. Ng, P.M. Polunin, Y.Chen, I.B. Flander, S.W. Shaw, M.I. Dykman, T.W. Kenny, "Nonlinearity of Degenerately Doped Bulk-Mode Silicon MEMS Resonators," J. Microelectromech., vol. 25, no. 5, p. 859-869, Oct 2016.

[4] Y. Yang, E.J. Ng, V. Hong, C. H. Ahn, Y. Chen, E Ahadi, M. Dykman, and T.W. Kenny, "Measurement of the Nonlinear Elasticity of Doped Bulk-Mode MEMS Resonators," Solid-State Sensors, Actuators, and Microsystem Workshop, Hilton Head 2014, pp. 285-288, Jun 2014.

[5] H. Zhu, G.C. Shan, C.H. Shek, and J.E.-Y Lee, "Shear dependent nonlinear vibration in a high quality factor single crystal silicon micromechanical resonator," Appl. Phys. Lett., vol. 101, no.3, p.034102, 2012.

[6] M.Shahmohammadi, H.Fatemi, and R. Abdolvand, "Nonlinearity reduction in silicon resonators by doping and re-orientation," in Proc. IEEE Int. Conf. Micro Electro Mech. Syst. (MEMS), Jan. 2013, pp. 793-796

[7] V. Kaajakari, T. Mattila, A. Lipsanen, and A. Oja, "Nonlinear mechanical effects in silicon longitudinal mode beam resonators," Sens. Actuators A, Phys., vol 120, no. 1, pp. 64-70, 2005.

[8] P. Polunin, Y. Yang, J. Atalaya, E. Ng, S. Strachan, O. Shoshani, M. Dykman, S. Shaw, and T. Kenny, "Characterizing MEMS Nonlinearities Directly: The Ring-Down Measurements," 2015 Transducers – 2015 18th International Conference on Solid-State Sensors, Actuators, and Microsystems (TRANSDUCERS), pp. 2176-2179, Jun 2015.

[9] E A. Partridge and M. Lutz, "Epi-seal pressure sensor and method for making an episeal pressure sensor", U.S. Patent 6928879, 2005., U.S. Patent 6928879, 2005.

[10] E. J. Ng, Y. Yang, Y. Chen, and T. W. Kenny, "An Etch Hole-Free Process for Temperature-Compensated High Q, Encapsulated Resonators", Solid-State Sensors, Actuators, and Microsystems Workshop, Hilton Head Isl., S.C., 6/8-6/12 (2014), pp. 99-100

[11] L.D. Landau and E.M. Lifshitz, Mechanics. Oxford, U.K.: Butterworth, 1976

[12] A.H. Nayfeh and D.T. Mook, Nonlinear Oscillators. New York, NY, USA: Wiley, 2007.

[13] H.K. Lee, R. Melamud, S. Chandorkar, J. Salvia, S. Yoneoka, and T.W. Kenny, "Stable operation of MEMS oscillators far above the critical vibration in the nonlinear regime," J. Microelectromech. Syst., vol. 20, no.6, pp.1228-1230, 2011.

[14] EL-CAT. INC. Properties of Silicon and Silicon Wafers: Resistivity & Mobility Calculator, accessed Mar 2019. [Online]. Available: https://www.el-cat.com/silicon-properties.html

CONTACT

*S.Koppaka,tel:+1-773-273-1240;skoppaka@stanford.edu